Results in Engineering 18 (2023) 101221

Contents lists available at ScienceDirect

Results in Engineering

journal homepage: www.sciencedirect.com/journal/results-in-engineering

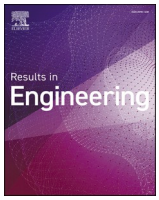

Seismic fragility analysis of low-rise unreinforced masonry buildings subjected to near- and far-field ground motions

Amirhosein Shabani [a,*], Maria Zucconi [b], Delaram Kazemian [c], Mahdi Kioumarsi [a]

[a] Department of Built Environment, Oslo Metropolitan University, Pilestredet 35, 0166, Oslo, Norway
[b] Department of Engineering, University Niccolò Cusano, Via Don Carlo Gnocchi, 3, 00166, Rome, Italy
[c] Department of Civil Engineering, Norwegian University of Science and Technology, Høgskoleringen 1, 7034, Trondheim, Norway

ARTICLE INFO

Keywords:
Low-rise buildings
Seismic fragility
Unreinforced masonry
Near-field ground motions
Pulse-like ground motions

ABSTRACT

Unreinforced masonry (URM) is considered one of the most cost-effective structural typologies for low-rise buildings in seismic regions. Near-field (NF) ground motions are sometimes characterized by high-velocity pulses that are typically more destructive than far-field (FF) seismic events. Therefore, a seismic fragility analysis of low-rise URM building typologies subjected to NF and FF seismic events was performed. Four URM walls were chosen, and nonlinear models of the walls were developed based on the double-modified, multiple vertical line element model (DM-MVLEM). The zero-moment coefficient was used to determine the effective uncracked section length of a pier. This parameter must be calculated for each pier of a perforated URM wall to derive the maximum shear strength of the piers using a nonlinear model development process. A simplified analytical method was proposed to obtain the zero-moment coefficient factor of piers by performing linear static analysis on nine perforated walls and regression analyses of the results. Subsequently, nonlinear pushover analysis was performed to derive the capacity curves, and the damage limit states were defined for each model according to the Eurocode 8 standard. Subsequently, incremental dynamic analysis (IDA) was performed for each case study by applying FF and NF ground motions. Finally, fragility curves were developed based on the IDA results for each damage limit state. The susceptibilities of one- and two-story URM walls subjected to FF and NF seismic events were investigated by examining the derived fragility curves.

1. Introduction

Recent earthquakes revealed the high vulnerability of unreinforced masonry (URM) buildings to seismic loads [1–3]. URM buildings constitute one of the oldest structural systems built without considering modern seismic design criteria [4]. Furthermore, the brittle material type with low-tensile strength and large mass, and the lack of connection between the walls and ceilings are other reasons for the high susceptibility of this structural typology to earthquake events [5,6]. URM is considered a prevalent structural system in high-seismicity zones and historic areas [7]. Furthermore, URM is considered to be one of the most popular and cost-effective structural systems for constructing low-rise buildings [8–10]. Therefore, seismic vulnerability assessment and the proposal of a strengthening strategy are required to improve the resiliency of this structural typology and sustainable reconstruction of historic areas.

Various methodologies have been proposed for the nonlinear modeling of URM structures, which can be categorized into 1) the discrete element method, 2) the continuum homogenous method, and 3) the equivalent frame method (EFM) [11,12]. The discrete element method is usually utilized for the nonlinear modeling of URM structural elements owing to its high-computational effort [13]. The continuum homogeneous method is typically utilized to model URM structures with complex architectures, such as churches, towers, or bridges [14,15]. However, various EFMs have been developed and are usually used for the nonlinear modeling of URM residential buildings with the lowest computational effort compared with the other two methods [16–18].

EFMs facilitate the performance of highly computationally demanding nonlinear dynamic analysis of URM buildings to obtain fragility curves [19–21]. Simulation-based analytical fragility curves more accurately represent damage probabilities than curves derived using simplified analytical, empirical, or hybrid methodologies [4]. The

* Corresponding author.
E-mail addresses: Amirhose@oslomet.no (A. Shabani), maria.zucconi@unicusano.it (M. Zucconi), delaramk@ntnu.no (D. Kazemian), Mahdik@oslomet.no (M. Kioumarsi).

https://doi.org/10.1016/j.rineng.2023.101221
Received 12 March 2023; Received in revised form 31 May 2023; Accepted 4 June 2023
Available online 5 June 2023

analytical fragility curves of URM buildings, which show the probability of exceeding a damage limit state for a structure subjected to an earthquake with a specific intensity measure (IM), can be obtained based on cloud analysis, multi stripe analysis, and incremental dynamic analysis (IDA) [8,22–25]. In these approaches, various seismic records with different intensities are applied to the model to evaluate the structural response [26]. IDA has the highest computational demand among the aforementioned methods; however, simplicity of implementation and no prior assumptions for the probabilistic distribution of seismic demand for the derivation of fragility functions are the two main advantages of this method [27,28].

The seismic events that were recorded and applied to a model for dynamic analysis were categorized into 1) far-field (FF), 2) pulse-like near-field, and 3) non-pulse-like near-field based on the site-to-source distance and presence of strong velocity pulses [29]. High-amplitude long-duration acceleration or velocity pulses occurring primarily in the fault-normal direction are the main characteristics of pulse-like near-field (NF) ground motions [30]. The main cause of pulses is the forward directivity effect, which typically occurs at sites in the direction of rupture propagation when the rupture velocity is close to the shear-wave velocity [29]. Different methodologies have been developed to distinguish pulse-like ground motions [31–33], and various studies have emphasized the higher level of damage that can be imposed on structures compared with other ground motion types [34–37]. In one of the few studies concerning the seismic vulnerability assessment of URM buildings subjected to FF and NF excitations, a three-dimensional (3D) one-story URM building was modeled, and it was concluded that the model was more susceptible to NF seismic events than FF ground motions [38]. Most studies concerning the effect of NF ground motions on the seismic behavior of URM buildings are limited to the pushover analysis of detailed numerical models and nonlinear time history analysis of the equivalent single-degree-of-freedom model of buildings [39,40]. However, equivalent single-degree-of-freedom models do not accurately reflect the seismic behavior of URM walls compared with the aforementioned numerical modeling approaches [4]. Therefore, a comparative study of the effects of NF and FF ground motions on the seismic fragility of URM buildings is required to develop sufficiently accurate numerical models and perform nonlinear dynamic analyses.

In this study, the macroelement utilized for the nonlinear modeling of URM case studies is first introduced. Subsequently, a simplified analytical method is proposed to calculate the maximum lateral strength (V_m) of the URM piers of a perforated URM wall. The proposed simplified analytical method enhances the efficiency of the nonlinear modeling process. This study was dedicated to the seismic fragility analysis of low-rise URM buildings. Unlike previous studies, this study employs detailed nonlinear modeling with the double-modified, multiple vertical line element model (DM-MVLEM) to capture accurately the complex behavior of URM walls. Four low-rise URM-perforated walls were chosen as case studies, and nonlinear models were constructed. Pushover analyses were performed, and the damage limit states were calculated for each case study. Subsequently, IDA was performed by applying FF and NF excitations to the case studies. The selected NF ground motions were pulse-like excitations used to investigate the pulse effects on the seismic behavior of the buildings. Finally, the fragility curves of each case study subjected to three seismic events were produced to facilitate a comparison of the seismic responses of the case studies. By conducting IDA and developing fragility curves, this study aims to enhance the understanding of the seismic response and vulnerability of low-rise URM buildings, thus contributing to effective strengthening strategies.

2. Case studies and nonlinear modeling

2.1. Case studies

The selected case studies were limited to low-rise URM walls with a maximum of two stories. Four perforated URM walls were selected as representatives of different structural typologies. Case study A was a wall tested at the University of Pavia subjected to prescribed cyclic displacements on the first and second floors [41]. The wall was made of solid fired-clay brick, and the mortar was a mixture of hydraulic lime and sand [41]. Case study B involved a two-story URM wall with five openings. Case studies C and D involved one-story URM walls with three and four openings, respectively. The four case studies and their geometries are shown in Fig. 1. All walls have a thickness of 25 cm and are made of the same material as the Pavia door wall [41].

2.2. Development of nonlinear models

3D modeling is necessary to predict the actual seismic behavior of buildings owing to the unpredictability of the seismic loading direction. Moreover, the asymmetry of the rigidity and mass distributions of each component with respect to the loading direction could be accurately predicted by performing 3D analyses. However, for simplicity, two-dimensional (2D) models were developed in this study that focused on horizontal motion in a single plane. These models suit buildings with simple plan forms that lack mass or stiffness cross-coupling between orthogonal horizontal directions [8]. Despite this simplification, it is believed that essential in-plane structural behaviors can be adequately represented. The main objective of this study was to compare intensively the analytical fragility curves obtained computationally from IDA. Hence, a 2D modeling strategy that disregards the out-of-plane behavior of walls but accurately depicts the in-plane behavior of structural elements has been adopted [18].

The geometry of the piers and spandrels was determined based on the Dolce method [42], which is defined as the most reliable method for the equivalent frame idealization of perforated URM walls [43]. Based on this method, spandrels and piers are connected with rigid elements such that the length of the spandrels equals the length of the openings. The effective height of the piers is derived from the intersection between the vertical centroidal axis of each pier and the lines forming a 30° angle from the corners of the adjacent openings [42]. The DM-MVLEM was used to develop the nonlinear models of the case studies [18]. The DM-MVLEM is a macroelement for the nonlinear analysis of URM buildings composed of two modified MVLEM elements to simulate the flexural behavior and a nonlinear shear spring that connects the modified MVLEM elements to simulate the shear behavior of URM structural components [18,20,44]. The DM-MVLEM was verified by comparing the results of the tests to the numerical analysis of two piers, a spandrel, and a full-scale two-story URM wall subjected to cyclic loading [18]. To accelerate the modeling procedure and reduce human errors, Hyperomet was utilized for the nonlinear modeling of walls based on the DM-MVLEM [45]. Hyperomet is a graphical user interface for the OpenSees software framework [46] designed for the nonlinear modeling of URM walls [45]. Fig. 2 depicts all the models developed using the DM-MVLEM macroelement.

The stress–strain curve of the URM material is depicted in Fig. 3(a), with a diagonal tensile strength (f_{td}) of 0.21 MPa and shear strength of the masonry at zero compressive stress (f_{v0}) of 0.345 MPa based on [41]. The strain–stress curve was assigned to the fibers of the DM-MVLEM, and a nonlinear material with a trilinear backbone curve was assigned to the nonlinear shear springs in the middle of the DM-MVLEMs [18]. Fig. 3(b) shows the typical backbone curve of a nonlinear shear spring. The lateral strength parameters of the curve are proportional to V_m and the corresponding displacements are proportional to the initial in-plane shear stiffness and height of the elements, as described in Ref. [18].

V_m is considered as the minimum value of the maximum lateral strength owing to the shear sliding (V_S) and diagonal cracking (V_D) failure modes calculated using Equations (1) and (2) [18].

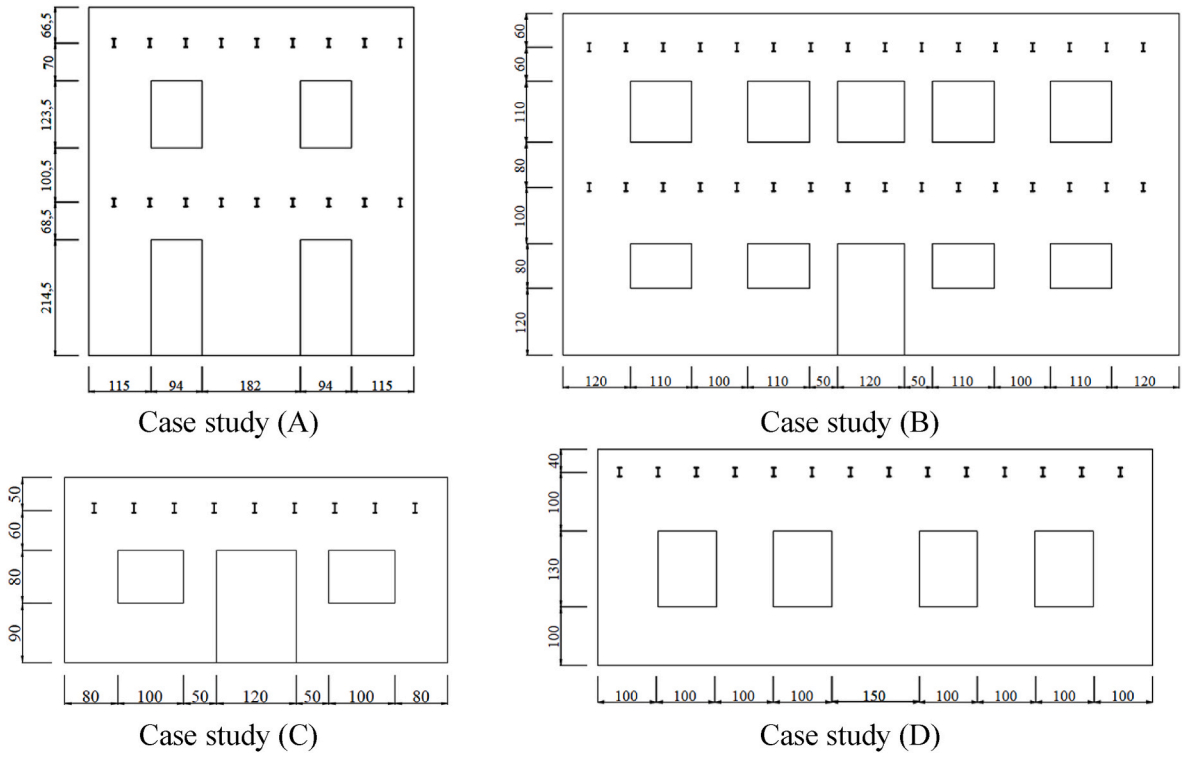

Fig. 1. Four low-rise URM walls as case studies.

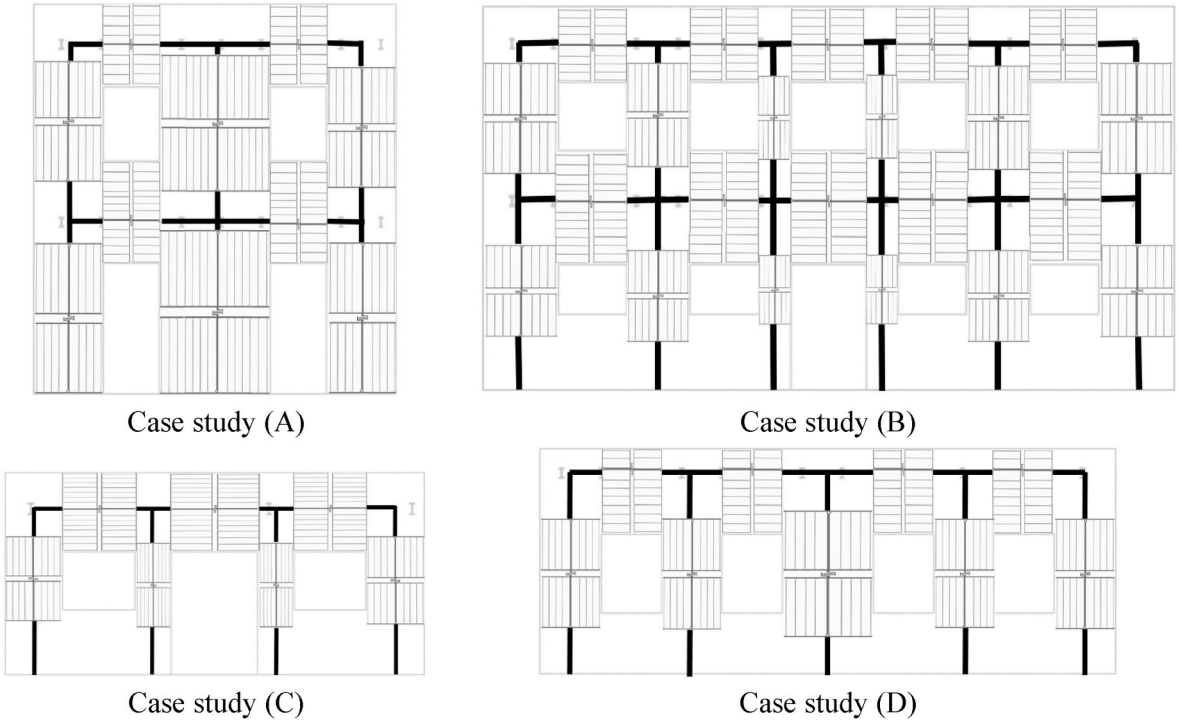

Fig. 2. Developed nonlinear models of the four case studies using DM-MVLEM macroelement.

$$V_S = \left(\frac{f_{td} + 0.4\sigma_0}{1 + \frac{3a_0 h f_{t0}}{\sigma_0 b}} \right) bt \quad (1)$$

$$V_D = \frac{f_{td} bt}{\zeta} \sqrt{1 + \frac{\sigma_0}{f_{td}}} \quad (2)$$

where b is the width, h is the height, and t is the thickness of a pier, is the axial compression stress, and ζ is the shear stress distribution coefficient at the center of a pier considering the aspect ratio calculated based on

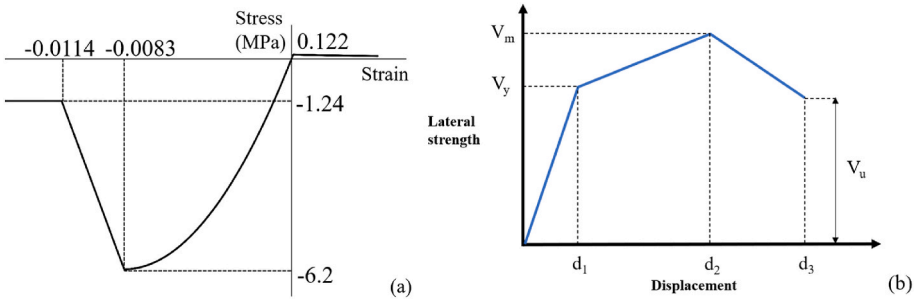

Fig. 3. (a) Stress–strain curve of URM and (b) trilinear backbone curve of the nonlinear shear spring.

the equations in Table 1:

Moreover, parameter α_0 is the zero-moment coefficient relevant to the moment distribution along the height of the pier, which is elaborated on in the next section.

2.3. Zero-moment coefficient

The zero-moment coefficient was calculated to determine the effective uncracked section length of a pier, neglecting the tensile strength of the bed joints and assuming a simplified distribution of compression stresses [47]. The parameter was utilized to calculate the V_S of the piers, as shown in Equation (1). The parameter α_0 is calculated as the maximum value of the fraction of the height of a pier (H_0) with a positive or negative moment value as depicted in Fig. 4 to the total height of a pier (h) [19]. For ideal typical test layouts, the α_0 is assumed to be equal to one in a cantilever scheme and 0.5 in a fixed-fixed boundary condition. No further description of this value is provided in Eurocode 8 Part 3 [48], NTC [49], FEMA 356 [50], or FEMA 273 [51]. This parameter depends on the geometry and boundary conditions of piers. Therefore, predefined ideal values cannot be assigned to α_0 of piers of a perforated URM wall due to the flexibility of spandrels on two ends of the pier.

One strategy is to apply a mode proportional load pattern based on the fundamental mode shape to the elastic model of the wall and define the moment distribution diagram of each pier and calculate α_0 [19]. However, different studies have indicated the accuracy of a pushover analysis of URM buildings with the mass-proportional load pattern compared with the mode-proportional load pattern by comparing the results with the IDA curves [18,52,53]. Therefore, in this study, the parameter α_0 was calculated by applying a mass-proportional lateral loading to the elastic model of the walls.

To investigate the variation in this parameter and define the equations that facilitate the process of attaining this parameter for the analysis of low-rise URM buildings, nine perforated URM walls were modeled in SAP 2000, considering the elastic behavior of piers and spandrels. The five added URM walls are illustrated in Fig. 5.

Mass-proportional lateral loads were applied to the case studies and the α_0 values were determined based on the moment diagram. The results show that the α_0 values of the piers of the two sides of the walls of the first story are higher than the values of the internal piers. Furthermore, if a load was applied in the right direction, the α_0 value of the leftmost pier was higher than that of the external pier. However, because the seismic events applied cyclic loads to the structures, the highest α_0 value was considered for both external piers using a more conservative approach.

To determine an equation to derive the α_0 values, the piers are subcategorized into three groups: 1) internal piers of the first story, 2) external piers of the first story, and 3) piers of the second story. The differences between the α_0 values of the interior and exterior piers of the second story were not as high as those of the first story; therefore, no distinction was considered. The piers of the one-story walls were assigned to groups 1 and 2. Moreover, $\frac{b^3}{h}$ was considered a parameter proportional to the flexural stiffness of each pier, depending on the geometry of each pier utilized for the prediction of the parameter α_0. Fig. 6 shows the diagrams of the α_0 versus $\frac{b^3}{h}$ for all three subcategories of all piers in the nine case studies. The log-normal trendlines were utilized to determine the prediction equations. The range of the calculated α_0 values, equations that can be used for the prediction of the parameter α_0 and the corresponding coefficient of determination (R^2) values are listed in Table 2. The range of the parameter shows that assuming fixed-fixed boundary conditions for the piers of the first story of a two-story perforated wall which corresponds to 0.5 for the parameter α_0 will overestimate the V_m of the piers since the calculated α_0 are more than 0.5, as presented in Table 2. Furthermore, assuming cantilever piers on the second floor of a two-story wall or piers of a one-story wall and assigning the value of one to the parameter α_0 will underestimate the V_m values of the piers.

Finally, to investigate the accuracy of the proposed equations, the V_m values of all piers of the nine walls were calculated using the α_0 values derived from the equations in Table 2 and the linear static analysis of the walls. A scatter plot of the results of the two approaches is shown in Fig. 7. The maximum R^2 value in Table 2, which shows the correlation of the calculated α_0 values based on the equations and numerical analysis is 75.78%. However, the R^2 value, which shows the correlation of the calculated V_m values is 99.95%, and the negligible deviation of the equality line from the best-fitted linear trendline indicates the robustness of the proposed simplified analytical method. Despite the relatively high dispersion between the predicted and exact α_0 values, the predicted and exact V_m values were similar. It is worth mentioning that the equations can only be used to define the α_0 parameter of the piers of the low-rise URM wall (maximum two-story) with a regular opening configuration; in other cases, static analysis is recommended (by applying the mass-proportional lateral load) instead of using fixed values from the codes.

Table 1
Equations used to derive ζ (the shear stress distribution coefficient at the center of a pier considering the aspect ratio).

Aspect ratio	Shear stress distribution coefficient
$\frac{h}{b} \leq 1 \rightarrow$	$\zeta = 1$
$1 < \frac{h}{b} < 1.5 \rightarrow$	$\zeta = \frac{h}{b}$
$\frac{h}{b} \geq 1.5 \rightarrow$	$\zeta = 1.5$

3. Pushover analysis

Pushover analysis was performed by applying the mass-proportional load pattern, and the pushover curves are illustrated in Fig. 8. Furthermore, for the Pavia door wall, a pushover curve derived by applying a load pattern similar to that in the test and the backbone of the test result were presented to demonstrate the accuracy of the DM-MVLEM method, as shown in Fig. 8(a). Although a difference can be detected between the

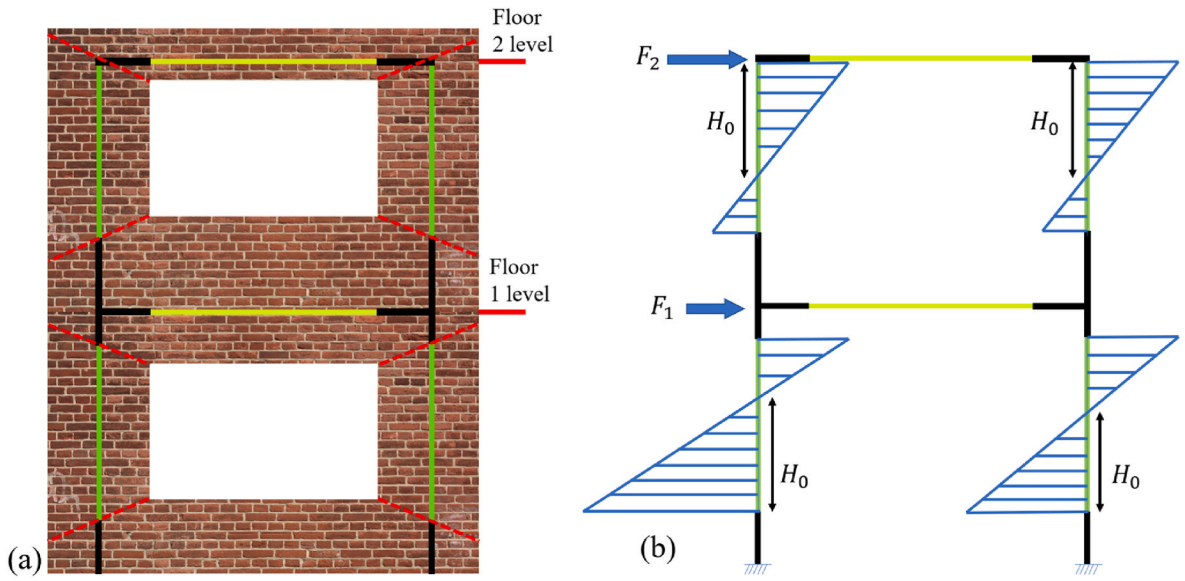

Fig. 4. (a) A perforated two-story URM wall and (b) the moment diagram of the wall subjected to lateral loadings and definition of H_0.

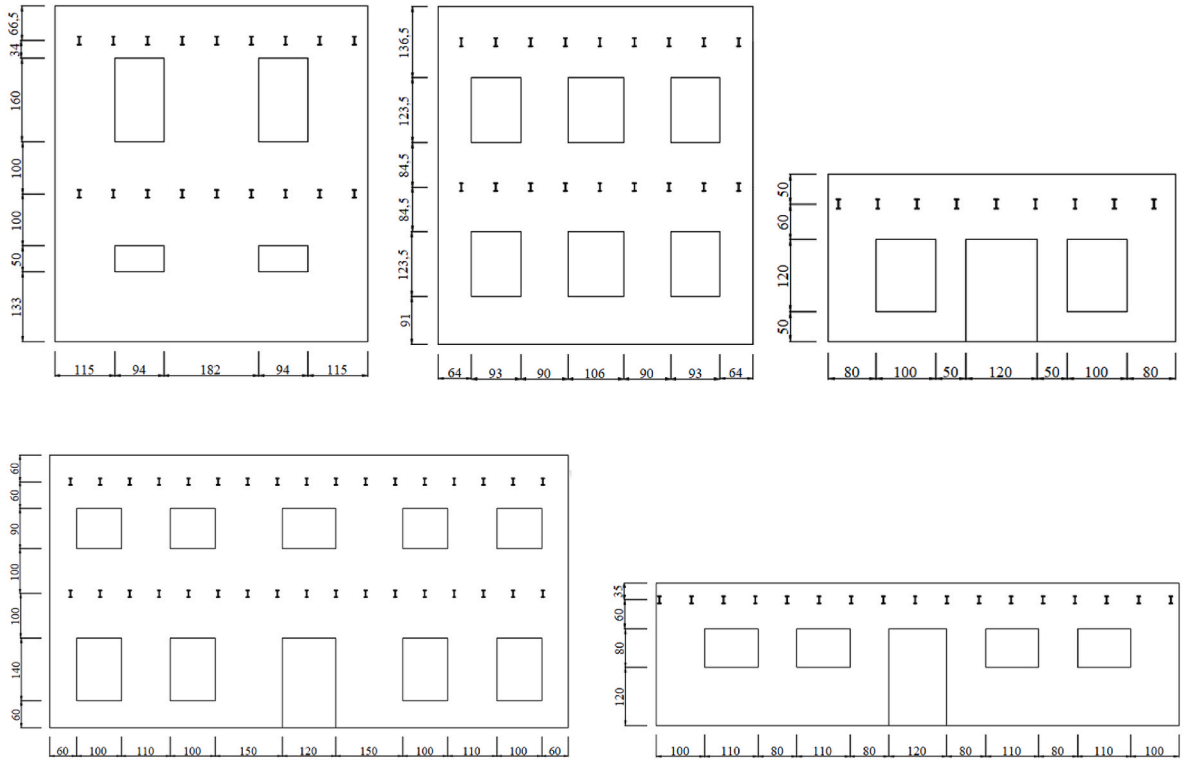

Fig. 5. Added five case studies chosen for the evaluation of the zero-moment coefficient factor.

initial stiffness of the test and the numerical model curves, the maximum base shear is predicted with good accuracy, and the nonlinear behavior, evaluated in terms of ductility, was estimated accurately. Note that the vertical applied load of the Pavia door wall was based on the test, but for other case studies, a uniform load (set at 20 $\frac{kN}{m}$) was applied to each floor, which is relatively lower than the vertical load applied to the Pavia door wall [41]. It can be inferred from Fig. 8 that the inclusion of piers or extension of the wall length, as seen in the two-story walls, leads to an increase in the maximum base shear for the one-story walls. The combined flexural and shear failure mode is the dominant failure mode of the piers in the case study (A), which can be concluded from the pushover curve analysis and is consistent with the test results. However, the shear failure mode is more dominant in other case studies. Therefore, the ductility of the case study (A) is greater than that of the other case studies.

3.1. Definition of limit states

Instead of considering predefined damage limit state values, a more accurate structure-specific approach based on the pushover curve was used to derive the inter-story drifts corresponding to the limit states [54]. Qualitative and quantitative descriptions of the three limit states

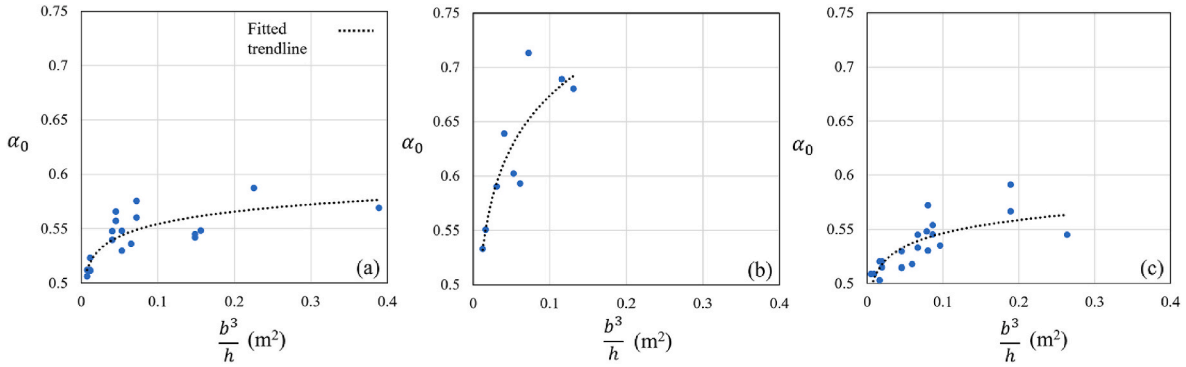

Fig. 6. Regression analysis results and trendlines of the data derived from analysis of (a) internal piers of the first story, (b) external piers of the first story, and (c) piers of the second story.

Table 2
Range of the calculated α_0 values, derived equations, and R^2 values for the piers in different positions.

Pier position	Range of α_0	Equation	R^2 (%)
Internal piers of the first story	$0.51 \leq \alpha_0 \leq 0.58$	$\alpha_0 = 0.0163 \ln\left(\frac{b^3}{h}\right) + 0.5919$	65.45
External piers of the first story	$0.53 \leq \alpha_0 \leq 0.71$	$\alpha_0 = 0.0677 \ln\left(\frac{b^3}{h}\right) + 0.8299$	75.78
Piers of the second story	$0.5 \leq \alpha_0 \leq 0.59$	$\alpha_0 = 0.0169 \ln\left(\frac{b^3}{h}\right) + 0.5834$	62.62

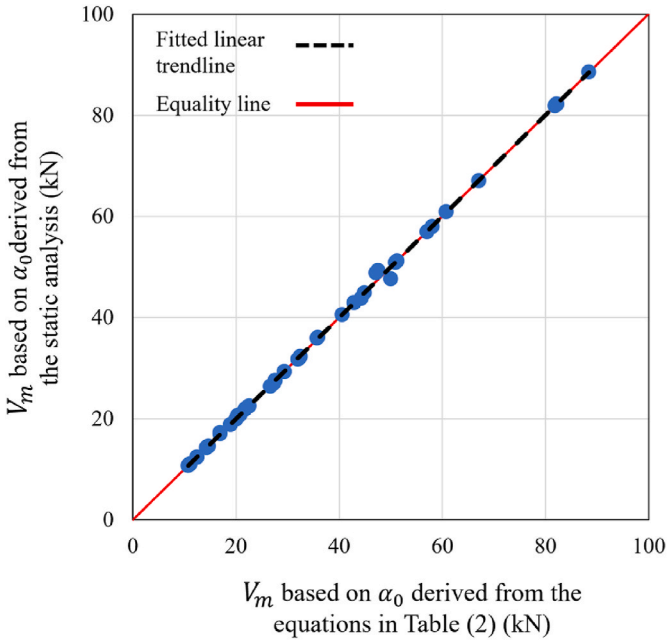

Fig. 7. Scatter plot and equality line for the results of the V_m based on α_0 derived from the static analysis and proposed equations.

selected based on Eurocode 8 Part 3 [48] are presented in Table 3.

The yielding points of the pushover curves were calculated after bilinear-elastic–perfectly plastic idealization of the pushover curves performed following the procedure recommended by Eurocode 8 part 1 [55] and using the SPO2FRAG user interface [56]. The yielding displacement was calculated by defining the area-balancing criterion between the area under the capacity curve and the idealized curve, and the corresponding maximum inter-story drift was considered as the damage limitation (DL) limit-state definition.

The ultimate displacement that corresponds to the near collapse (NC) limit state was calculated when the pushover analysis stopped converging, or the corresponding displacement was 80% of the peak base shear [56]. Furthermore, the significant damage (SD) limit state was estimated as the maximum inter-story drift corresponding to 75% of the ultimate displacement value, which approximately corresponds to the displacement of the maximum base shear [57].

The limit state values are influenced by the dominant failure modes of the piers, which are dependent on the opening configurations that affect the geometry of the piers and spandrels and the applied vertical loads, as highlighted in Refs. [57,58]. The differences between the calculated inter-story drifts corresponding to each limit state of the walls are shown in Fig. 9. Therefore, structure-specific methods for deriving the limit states of URM buildings are recommended instead of using predefined values from the literature, although for cases B, C, and D, the obtained values are similar. These results highlight the need to investigate this issue further to identify fixed values of the damage states according to specific structural features.

4. Incremental dynamic analysis

The Rayleigh damping model was implemented with an equivalent damping ratio of 2% at the first and second modal frequencies of each model [18,59,60]. Considering the convergence issues and prolonged analysis associated with using the current stiffness matrix, it may be advisable to replace it with a committed stiffness matrix [61]. This alternative results in significant computational time savings. Therefore, Rayleigh damping was incorporated based on the mass and last committed stiffness matrix to perform IDA.

IDA was performed by applying 22 FF and 14 NF pairs of seismic records from FEMA P695 [62]. A boundary of 10 km was considered to categorize the records into FF and NF [62]. The average of the Campbell and Joyner–Boore fault distances was used as the source-to-site distance. NF records were selected based on the three criteria mentioned in Ref. [31]. Wavelet analysis was used to extract the largest velocity pulse from a given ground motion. The presence of a pulse that occurs early in the time history is satisfied by calculating an indicator and checking the

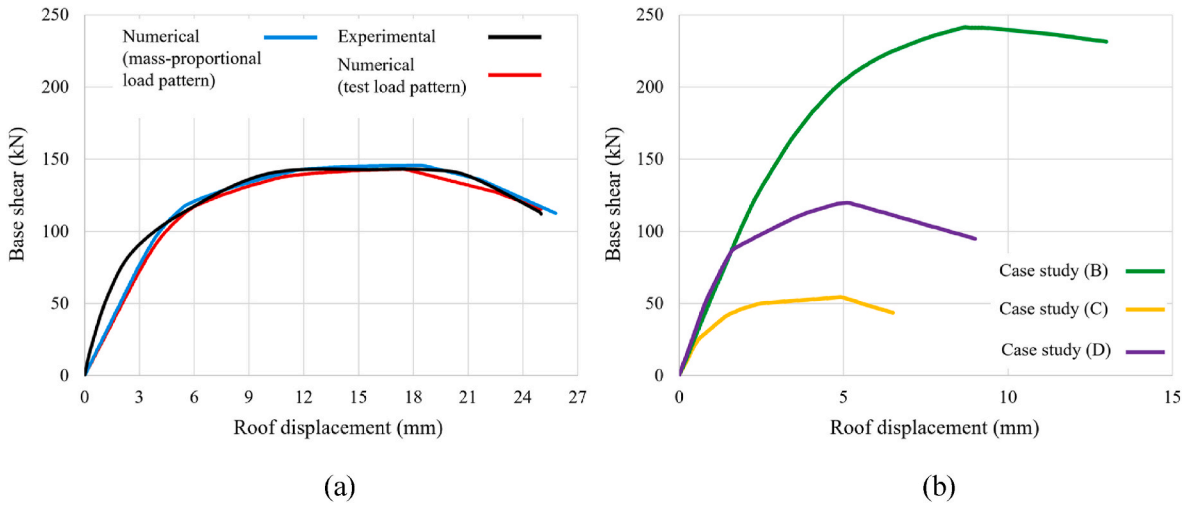

Fig. 8. Pushover curves of (a) case study (A) (Pavia door wall) with the test results, and (b) other case studies.

Table 3
Quantitative and qualitative descriptions of defined three performance levels [48].

Description type	Performance levels		
	Damage limitation	Significant damage	Near collapse
Qualitative description	Building is considered as slightly damaged. Sustain minimal or no damage to their structural elements and only minor damage to their nonstructural components	Building is considered as significantly damaged—extensive damage to structural and non-structural components	Building is considered as heavily damaged. Experience a significant hazard to life safety resulting from the failure of non-structural components
Quantitative description	Yielding point of the idealized bilinear capacity curve	75% of the ultimate top displacement capacity	Maximum displacement corresponds to 80% of the peak base shear

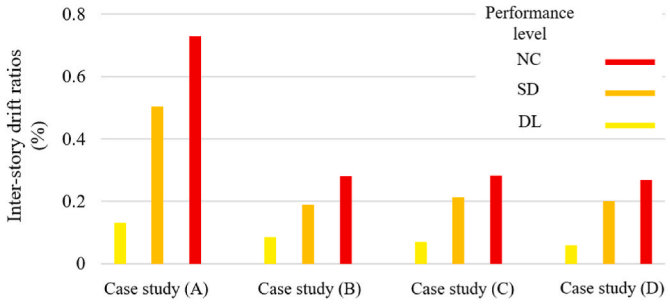

Fig. 9. Determined limit states for the case studies from the pushover analysis.

pulse occurrence time [31]. Another criterion is that the ground motion should have a PGV greater than 30 cm/s . The occurrence of an early pulse in the ground motion was independent of the scaling process of the IDA. However, a PGV greater than 30 cm/s may not be satisfied for ground motions scaled to intensities lower than the original ground motion. Therefore, the PGV criterion was neglected in this study because of the downscaling process of the IDA. A summary of the ground motions selected from FEMA P695 [62] and their characteristics, including the record sequence numbers (RSN) in the PEER database [63] and the maximum peak ground acceleration (PGA) of the two components of each earthquake, are presented in Table 4. The FF and NF ground motions' spectra are shown in Fig. 10.

An IDA curve is a diagram of the ground motion IM against an engineering demand parameter (EDP) [28,65]. In this study, the IM is the spectral acceleration corresponding to the first mode of the structure considering 5% of damping (Sa (T_1, 5%)), and EDP is the maximum inter-story drift. Note that the fundamental period of the two-story walls (case studies (A) and (B)) was 0.21 s. The fundamental periods of one-story walls were 0.12 s and 0.13 s for case studies (C) and (D), respectively. The IDA curves for the case studies are shown in Fig. 11.

5. Seismic fragility analysis

A log-normal cumulative distribution function was used to define the fragility function based on Equation (3).

$$P[C|IM = im] = \Phi\left[\frac{ln(im) - \eta}{\beta}\right] \quad (3)$$

where $P[C|IM = im]$ is the probability that a ground motion with $IM = im$ causes the structure to collapse. $\Phi()$ is the standard normal cumulative distribution function, ln (Z) is the natural logarithm function, η and β are the mean and standard deviation of the ln*(im)* values, respectively [66,67].

The fragility curves were produced based on the results from the IDA, considering together all 72 time-history analyses. The analyses outcomes related to the FF and those related to the NF seismic events for all three mentioned limit states are presented, as shown in Fig. 12. Unlike the fragility curves for the DL limit state, the fragility curves for the NC and SD limit states are close to each other. This is in part due to the brittle behavior of URM material that causes a lower difference between the seismic demand when it is significantly or heavily damaged, especially for earthquakes characterized by a medium–high magnitude (Magnitude = 6.5–7.5 M), as in the cases if the selected ones (see Table 4). It can be concluded that case study (B) is the most vulnerable case study, with the lowest IM corresponding to a 50% probability of reaching a limit state (median IM), whereas case study (D) yielded the opposite results.

The maximum difference between the median IMs of FF and NF ground motions is 6.2%. This corresponds to the case study (A), considering the Sa (T_1, 5%) as the IM. Therefore, it can be inferred that the seismic fragility analysis of low-rise URM buildings by applying FF

Table 4
Summary of earthquake events and recording station data for the FF and NF record sets [64].

Earthquake	Magnitude (M)	Year	FF ground motions			NF ground motions		
			Station	RSN	PGA_{max}	Station	RSN	PGA_{max}
Northridge	6.7	1994	Beverly Hills-Mulhol	953	0.52	Rinaldi Receiving Sta	1063	0.87
Northridge	6.7	1994	Canyon Country	960	0.48	Sylmar - Olive View	1086	0.73
Duzce, Turkey	7.1	1999	Bolu	1602	0.82	Duzce	1605	0.52
Hector Mine	7.1	1999	Hector	1787	0.34	–	–	
Imperial Valley	6.5	1979	Delta	169	0.35	El Centro Array #6	181	0.44
Imperial Valley	6.5	1979	El Centro Array #11	174	0.38	El Centro Array #7	182	0.46
Kobe, Japan	6.9	1995	Nishi-Akashi	1111	0.51	–	–	
Kobe, Japan	6.9	1995	Shin-Osaka	1116	0.24	–	–	
Kocaeli, Turkey	7.5	1999	Duzce	1158	0.36	Izmit	1165	0.22
Kocaeli, Turkey	7.5	1999	Arcelik	1148	0.22	–	–	
Landers	7.3	1992	Yermo Fire Station	900	0.24	Lucerne	879	0.79
Landers	7.3	1992	Coolwater	848	0.42	–	–	
Loma Prieta	6.9	1989	Capitola	752	0.53	Saratoga–Aloha	802	0.38
Loma Prieta	6.9	1989	Gilroy Array #3	767	0.56	–	–	
Manjil, Iran	7.4	1990	Abbar	1633	0.51	–	–	
Superstition Hills	6.5	1987	El Centro Imp. Co.	721	0.36	–	–	
Superstition Hills	6.5	1987	Poe Road (temp)	725	0.45	–	–	
Cape Mendocino	7	1992	Rio Dell Overpass	829	0.55	Petrolia	828	0.63
Chi-Chi, Taiwan	7.6	1999	CHY101	1244	0.44	TCU065	1503	0.82
Chi-Chi, Taiwan	7.6	1999	TCU045	1485	0.51	TCU102	1529	0.29
San Fernando	6.6	1971	LA - Hollywood Stor	68	0.21	–	–	
Friuli, Italy	6.5	1976	Tolmezzo	125	0.35	–	–	
Irpinia, Italy-01	6.9	1980	–	–		Sturno	292	0.31
Superstition Hills-02	6.5	1987	–	–		Parachute Test Site	723	0.42
Erzican, Turkey	6.7	1992	–	–		Erzincan	821	0.49

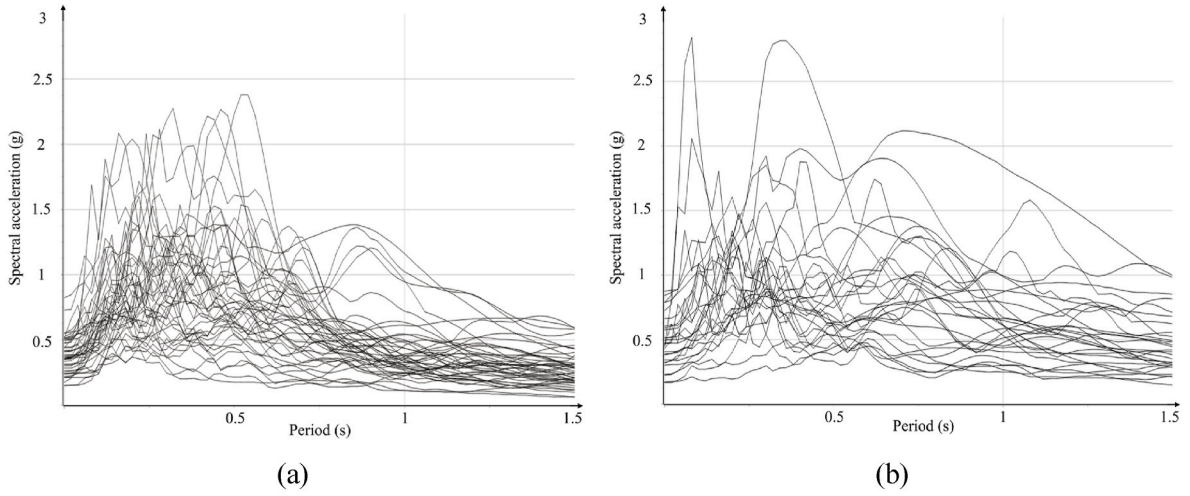

Fig. 10. (a) FF and (b) and NF ground motions' spectra.

and ignoring NF ground motions was sufficiently accurate for the selected case studies subject to strong ground motions. However, further investigations are required for seismic events characterized by medium intensities (Magnitude = 5.5–6.5 M).

Furthermore, the results showed that the median IMs of the NF ground motions applied to the two-story walls are lower than those of the FF seismic events. This difference is negligible in the case study (B). Nevertheless, for one-story buildings, the obtained results are the opposite. In one-story walls, the differences between the fragility curves of the FF are indistinguishable from those of the NF ground motions. It can be concluded that for two-story walls, the NF ground motions are more damaging than those for the FF motions; however, for one-story walls, the FF ground motions are more destructive. This difference shows that for the two-story walls with a fundamental period of 0.21 s, the NF records can impose more damages in terms of inter-story drifts. However, for one-story walls with a fundamental period of around 0.12 s, the FF seismic events are more damaging, which is consistent with the results of nonlinear analysis of stiff and low-period structures, such as masonry mosques [68], masonry bridges [69,70], and nuclear structures [71]. The NF ground motions caused more damage to the models with higher fundamental period values, which can be observed in the two-story walls.

A general rule that can exhibit the vulnerability of low-rise URM buildings cannot be determined because the seismic demand depends on the dynamic characteristics and failure modes of the structural elements. The same results were derived from a similar study on the seismic damage assessment of low-rise moderate reinforced concrete frames subjected to NF and FF ground motions [72]. Furthermore, it is mentioned that the derived fragility curves from both groups of ground motions are close to each other [72]. Applying NF ground motions is not required for the seismic fragility analysis of one-story URM buildings subjected to medium–high seismic events. Nonetheless, applying NF ground motions for the seismic fragility analysis of the two-story URM building mode is suggested for accurate analysis.

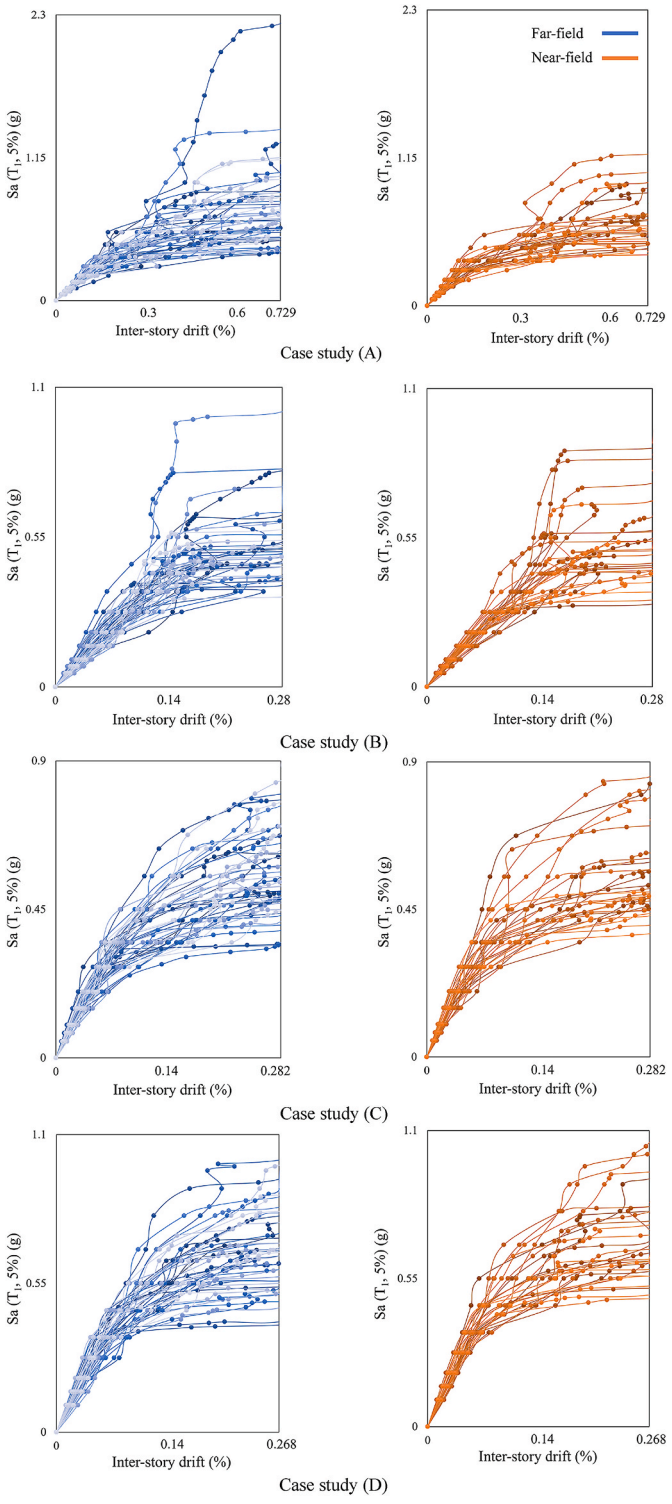

Fig. 11. IDA curves of the case studies subjected to FF and NF ground motions.

6. Conclusion

Because of the widespread use of low-rise (URM) buildings in high-seismic zones, this study aimed to evaluate the vulnerability in terms of the fragility curves of this structural system subjected to far-field (FF) and near-field (NF) ground motions. Four low-rise perforated URM walls were chosen, and nonlinear models were developed based on the double-modified multiple vertical line element model (DM-MVLEM). The maximum lateral strength (V_m) is an effective parameter on the trilinear backbone curve of the nonlinear shear spring of the DM-MVLEM macroelement, which is calculated based on the minimum value of the maximum lateral strength due to the shear sliding (V_S) and diagonal cracking (V_D) failure modes. Moreover, for the calculation of the V_S, the zero-moment coefficient (α_0) was required to be determined. The value of α_0 can be defined based on the moment diagram of each pier by applying lateral loads to a wall and performing linear static analysis. The main findings of this study can be synthesized as follows:

- A set of three equations was presented by performing regression analysis on the results of the linear static analysis of the nine walls. Comparison of the equality line and linear fitted trendline of the results of the V_m based on α_0 derived from the static analysis and proposed equations show the accuracy of the proposed simplified analytical method. Therefore, parameter α_0 can be derived based on the proposed equations instead of developing the linear equivalent frame model of the wall and performing static analysis. Furthermore, the results showed that using the α_0 values proposed for piers with ideal fixed or fixed-free boundary conditions was not sufficiently accurate for piers of a perforated wall with flexible boundary conditions owing to the presence of spandrels. Note that the proposed equations can only be used to define the parameter α_0 of the piers of a low-rise URM wall (maximum two-story) with regular opening configurations.
- A nonlinear pushover analysis was performed, and structure-specific damage limit states were calculated based on the pushover curves. The results showed that using predefined fixed inter-story drift ratios for the limit states of URM walls was not sufficiently robust. These differences were due to the different displacement capacities of the piers with shear or flexural failure modes.
- IDA was performed by applying 44 FF and 28 NF ground motions to the models, and the fragility curves for the three performance levels were obtained for each case study. The fragility curves for the NC and SD limit states were relatively close to each other, unlike the fragility curve for the DL limit state. The fragility curves revealed that the difference between the seismic demands of the buildings subjected to FF and NF ground motions was not significant for the low-rise URM buildings analyzed in this study. The maximum difference between the median IMs of FF and NF ground motions required to reach a limit state was 6.2%. This was achieved in case study (A), considering the Sa (T_1, 5%) as the IM. This behavior can be attributed to the brittle nature of the URM material, which results in a reduced disparity in seismic demand when the material is significantly or heavily damaged, especially for buildings subject to strong ground motions, such as those considered in this study, characterized by a magnitude in the range of 6.5–7.5 M.
- Thus, the seismic fragility analysis of low-rise URM buildings following the application of FF ground motions and the ignorance of NF ground motions is sufficiently accurate for medium-high-intensity seismic events. The study found that for two-story walls with a fundamental period of 0.21 s, the NF ground motions were more damaging than FF motions, while for one-story walls with a fundamental period of around 0.12 s, the FF ground motions were more destructive. Additionally, the fragility curves of the FF for one-story buildings were indistinguishable from those of the NF ground motions. Therefore, the use of NF ground motions was not necessary for the seismic fragility analysis of one-story URM buildings; however, for an accurate analysis of two-story URM buildings, NF ground motions should be included.

While efforts were made to encompass various opening configurations and geometries, additional case studies can be conducted to reduce further the uncertainty associated with the prediction of α_0. The comparative study procedure outlined in this study can also be extended to 3D models, considering the impact of irregular mass and stiffness in the plan and local collapse mechanisms. Additionally, investigating the

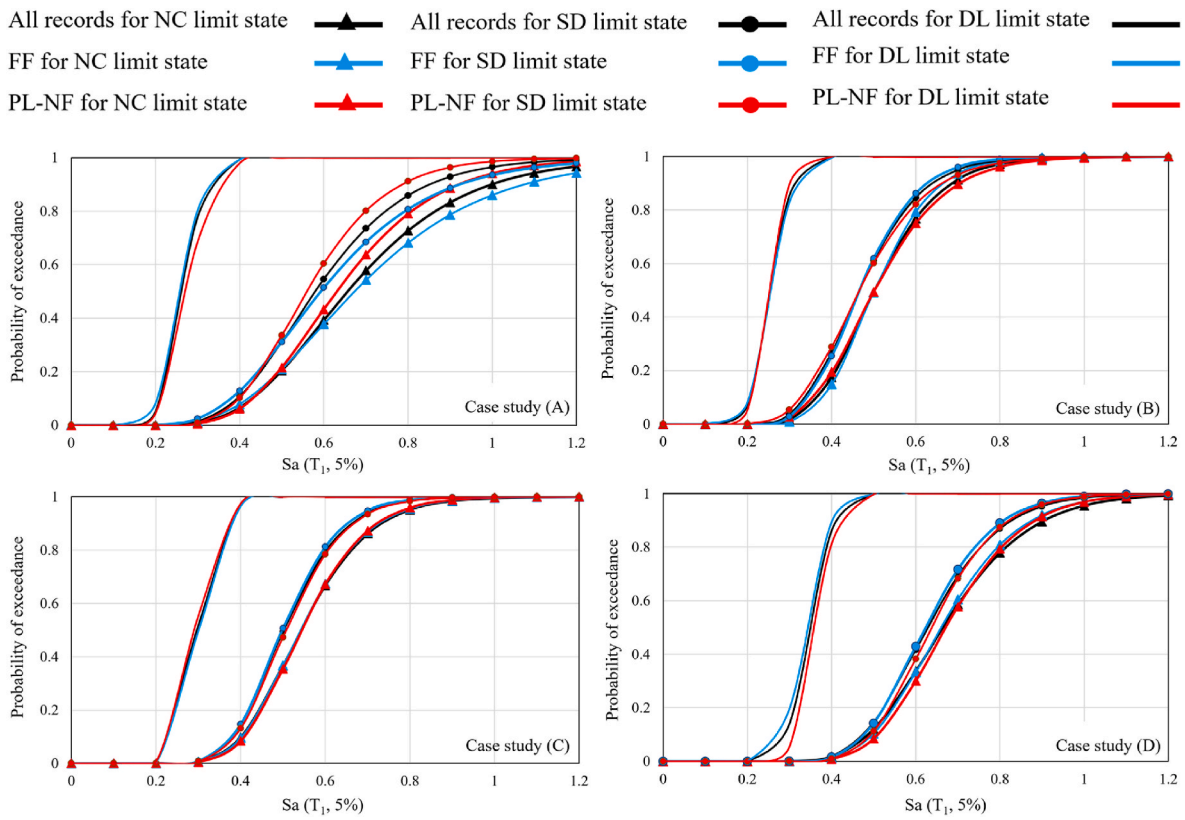

Fig. 12. Fragility curves of the case studies subjected to FF and NF ground motions for all three damage limit states for case studies A-D.

influence of different types of ground motion IM on seismic fragility curves could serve as a potential subject for future research.

Declaration of competing interest

The authors declare that they have no known competing financial interests or personal relationships that could have appeared to influence the work reported in this paper.

Data availability

No data was used for the research described in the article.

Acknowledgments

This work is a part of the HYPERION project. HYPERION has received funding from the European Union's Framework Programme for Research and Innovation (Horizon 2020) under grant agreement No 821054. The contents of this publication are the sole responsibility of Oslo Metropolitan University (Work Package 5, Task 2) and do not necessarily reflect the opinion of the European Union.

References

[1] M. Biglari, A. Formisano, Damage probability matrices and empirical fragility curves from damage data on masonry buildings after sarpol-e-zahab and bam earthquakes of Iran, Frontiers in Built Environment 6 (2020), https://doi.org/10.3389/fbuil.2020.00002.

[2] Z. Celep, A. Erken, B. Taskin, A. Ilki, Failures of masonry and concrete buildings during the march 8, 2010 kovancılar and palu (elazığ) earthquakes in Turkey, Eng. Fail. Anal. 18 (2011) 868–889, https://doi.org/10.1016/j.engfailanal.2010.11.001.

[3] M. Zucconi, M. Di Ludovico, L. Sorrentino, Census-based typological usability fragility curves for Italian unreinforced masonry buildings, Bull. Earthq. Eng. 20 (2022) 4097–4116, https://doi.org/10.1007/s10518-022-01361-8.

[4] A. Shabani, M. Kioumarsi, M. Zucconi, State of the art of simplified analytical methods for seismic vulnerability assessment of unreinforced masonry buildings, Eng. Struct. 239 (2021), 112280, https://doi.org/10.1016/j.engstruct.2021.112280.

[5] A. Aşıkoğlu, G. Vasconcelos, P.B. Lourenço, B. Pantò, Pushover analysis of unreinforced irregular masonry buildings: lessons from different modeling approaches, Eng. Struct. 218 (2020), 110830, https://doi.org/10.1016/j.engstruct.2020.110830.

[6] S. Colonna, S. Imperatore, M. Zucconi, B. Ferracuti, Post-seismic damage assessment of a historical masonry building: the case study of a school in teramo, Key Eng. Mater. 747 (2017) 620–627, https://doi.org/10.4028/www.scientific.net/KEM.747.620.

[7] M. Zucconi, R. Ferlito, L. Sorrentino, Typological damage fragility curves for unreinforced masonry buildings affected by the 2009 L'aquila, Italy earthquake, Open Civ. Eng. J. 15 (2021) 117–134, https://doi.org/10.2174/1874149502115010117.

[8] J. Park, P. Towashiraporn, J.I. Craig, B.J. Goodno, Seismic fragility analysis of low-rise unreinforced masonry structures, Eng. Struct. 31 (2009) 125–137, https://doi.org/10.1016/j.engstruct.2008.07.021.

[9] R. Marques, P.B. Lourenço, Unreinforced and confined masonry buildings in seismic regions: validation of macro-element models and cost analysis, Eng. Struct. 64 (2014) 52–67, https://doi.org/10.1016/j.engstruct.2014.01.014.

[10] P. Joyklad, Q. Hussain, Development of strength models for brick walls: experimental and theoretical study, Results in Engineering 18 (2023), 101103, https://doi.org/10.1016/j.rineng.2023.101103.

[11] A.M. D'Altri, V. Sarhosis, G. Milani, J. Rots, S. Cattari, S. Lagomarsino, et al., Modeling strategies for the computational analysis of unreinforced masonry structures: review and classification, Arch. Comput. Methods Eng. 27 (2020) 1153–1185, https://doi.org/10.1007/s11831-019-09351-x.

[12] T.M. Ferreira, N. Mendes, R. Silva, Multiscale seismic vulnerability assessment and retrofit of existing masonry buildings, Buildings 9 (2019) 91, https://doi.org/10.3390/buildings9040091.

[13] B. Pulatsu, S. Gonen, F. Parisi, E. Erdogmus, K. Tuncay, M.F. Funari, et al., Probabilistic approach to assess URM walls with openings using discrete rigid block analysis (D-RBA), J. Build. Eng. 61 (2022), 105269, https://doi.org/10.1016/j.jobe.2022.105269.

[14] A. Shabani, M. Skamantzari, S. Tapinaki, A. Georgopoulos, V. Plevris, M. Kioumarsi, 3D simulation models for developing digital twins of heritage structures: challenges and strategies, Procedia Struct. Integr. 37 (2022) 314–320, https://doi.org/10.1016/j.prostr.2022.01.090.

[15] A. Shabani, M. Feyzabadi, M. Kioumarsi, Model updating of a masonry tower based on operational modal analysis: the role of soil-structure interaction, Case Stud. Constr. Mater. 16 (2022), e00957, https://doi.org/10.1016/j.cscm.2022.e00957.

[16] M. Peruch, E. Spacone, G. Camata, Nonlinear analysis of masonry structures using fiber-section line elements, Earthq. Eng. Struct. Dynam. 48 (2019) 1345–1364, https://doi.org/10.1002/eqe.3188.

[17] S. Lagomarsino, A. Penna, A. Galasco, S. Cattari, TREMURI program: an equivalent frame model for the nonlinear seismic analysis of masonry buildings, Eng. Struct. 56 (2013) 1787–1799, https://doi.org/10.1016/j.engstruct.2013.08.002.

[18] A. Shabani, M. Kioumarsi, A novel macroelement for seismic analysis of unreinforced masonry buildings based on MVLEM in OpenSees, J. Build. Eng. 49 (2022), 104019, https://doi.org/10.1016/j.jobe.2022.104019.

[19] S. Petrovčič, V. Kilar, Seismic failure mode interaction for the equivalent frame modeling of unreinforced masonry structures, Eng. Struct. 54 (2013) 9–22, https://doi.org/10.1016/j.engstruct.2013.03.050.

[20] A. Shabani, M. Kioumarsi, Pros and cons of various equivalent frame models for nonlinear analysis of URM buildings, in: 8th European Congress on Computational Methods in Applied Sciences and Engineering ECCOMAS, 2022, p. 12.

[21] K. Demirlioglu, S. Gonen, S. Soyoz, M.P. Limongelli, In-plane seismic response analyses of a historical brick masonry building using equivalent frame and 3D FEM modeling approaches, Int. J. Architect. Herit. 14 (2020) 238–256, https://doi.org/10.1080/15583058.2018.1529208.

[22] K.R. Mackie, B. Stojadinović, Comparison of incremental dynamic, cloud, and stripe methods for computing probabilistic seismic demand models, Structures Congress (2005) 1–11, 2005.

[23] L. Su, X-l Li, Y-p Jiang, Comparison of methodologies for seismic fragility analysis of unreinforced masonry buildings considering epistemic uncertainty, Eng. Struct. 205 (2020), 110059, https://doi.org/10.1016/j.engstruct.2019.110059.

[24] L. Pasticier, C. Amadio, M. Fragiacomo, Non-linear seismic analysis and vulnerability evaluation of a masonry building by means of the SAP2000 V.10 code, Earthq. Eng. Struct. Dynam. 37 (2008) 467–485, https://doi.org/10.1002/eqe.770.

[25] P. Debnath, L. Halder, S. Chandra Dutta, Damage survey and seismic vulnerability assessment of unreinforced masonry structures in low-intensity Ambasa earthquake of northeast India, Structures 44 (2022) 372–388, https://doi.org/10.1016/j.istruc.2022.08.005.

[26] O. Souri, M. Mofid, Seismic evaluation of concentrically braced steel frames equipped with yielding elements and BRBs, Results in Engineering 17 (2023), 100853, https://doi.org/10.1016/j.rineng.2022.100853.

[27] L. Di Sarno, G. Karagiannakis, On the seismic fragility of pipe rack—piping systems considering soil–structure interaction, Bull. Earthq. Eng. 18 (2020) 2723–2757, https://doi.org/10.1007/s10518-020-00797-0.

[28] D. Vamvatsikos, C.A. Cornell, Incremental dynamic analysis, Earthq. Eng. Struct. Dynam. 31 (2002) 491–514.

[29] M. Kohrangi, D. Vamvatsikos, P. Bazzurro, Pulse-like versus non-pulse-like ground motion records: spectral shape comparisons and record selection strategies, Earthq. Eng. Struct. Dynam. 48 (2019) 46–64, https://doi.org/10.1002/eqe.3122.

[30] J.W. Baker, C.A. Cornell, Vector-valued intensity measures for pulse-like near-fault ground motions, Eng. Struct. 30 (2008) 1048–1057, https://doi.org/10.1016/j.engstruct.2007.07.009.

[31] J.W. Baker, Quantitative classification of near-fault ground motions using wavelet analysis, Bull. Seismol. Soc. Am. 97 (2007) 1486–1501.

[32] S.K. Shahi, J.W. Baker, An efficient algorithm to identify strong-velocity pulses in multicomponent ground motions, Bull. Seismol. Soc. Am. 104 (2014) 2456–2466.

[33] V. Dimakopoulou, M. Fragiadakis, I. Taflampas, A wavelet-based approach for truncating pulse-like records, Bull. Earthq. Eng. (2022) 1–24.

[34] F. Pugliese, L. Di Sarno, Probabilistic structural performance of RC frames with corroded smooth bars subjected to near- and far-field ground motions, J. Build. Eng. 49 (2022), 104008, https://doi.org/10.1016/j.jobe.2022.104008.

[35] H. Sha, X. Chong, L. Xie, P. Huo, T. Yue, J. Wei, Seismic performance of precast concrete frame with energy dissipative cladding panel system: half-scale test and numerical analysis, Soil Dynam. Earthq. Eng. 165 (2023), 107712, https://doi.org/10.1016/j.soildyn.2022.107712.

[36] F. Ahmad, A. Phillips, Buckling restrained braced frame seismic response for far-field, near-field, and long-duration earthquakes, J. Constructional Steel Res. 199 (2022), 107625, https://doi.org/10.1016/j.jcsr.2022.107625.

[37] A. Daei, M. Poursha, M. Zarrin, Seismic performance evaluation of code-compliant RC moment-resisting frame buildings subjected to near-fault pulse-like and non-pulse-like ground motions, J. Earthq. Eng. 26 (2022) 5058–5085, https://doi.org/10.1080/13632469.2020.1859003.

[38] A. Afreen, A. Ahmed, K. Moin, Effect of near-field earthquake on masonry structure, Asian Journal of Civil Engineering 22 (2021) 895–910, https://doi.org/10.1007/s42107-021-00353-4.

[39] H. Bilgin, M. Hysenlliu, Comparison of near and far-fault ground motion effects on low and mid-rise masonry buildings, J. Build. Eng. 30 (2020), 101248, https://doi.org/10.1016/j.jobe.2020.101248.

[40] M. Yekrangnia, A. Bakhshi, M.A. Ghannad, M. Panahi, Risk assessment of confined unreinforced masonry buildings based on FEMA P-58 methodology: a case study—school buildings in Tehran, Bull. Earthq. Eng. 19 (2021) 1079–1120, https://doi.org/10.1007/s10518-020-00990-1.

[41] G. Magenes, G. Kingsley, G. Calvi, Seismic Testing of a Full-Scale, Two-Story Masonry Building: Test Procedure and Measured Experimental Response Report 3.0, G.N.D.T. Department of Structural Mechanics, University of Pavia, 1995.

[42] M. Dolce, Schematizzazione e modellazione degli edifici in muratura soggetti ad azioni sismiche, in: L'industria Delle Costruzioni, vol. 25, 1991, pp. 44–57 (Italian).

[43] S. Cattari, A.M. D'Altri, D. Camilletti, S. Lagomarsino, Equivalent frame idealization of walls with irregular openings in masonry buildings, Eng. Struct. 256 (2022), 114055, https://doi.org/10.1016/j.engstruct.2022.114055.

[44] M. Kioumarsi, V. Plevris, A. Shabani, Vulnerability assessment of cultural heritage structures, in: 8th European Congress on Computational Methods in Applied Sciences and Engineering (ECCOMAS Congress 2022), ECCOMAS, 2022.

[45] A. Shabani, M. Kioumarsi, Hyperomet: an OpenSees interface for nonlinear analysis of unreinforced masonry buildings, SoftwareX 20 (2022), 101230, https://doi.org/10.1016/j.softx.2022.101230.

[46] S. Mazzoni, F. McKenna, M.H. Scott, G.L. Fenves, OpenSees command language manual, Pacific Earthquake Engineering Research (PEER) Center 264 (2006) 137–158.

[47] G. Magenes, G.M. Calvi, In-plane seismic response of brick masonry walls, Earthq. Eng. Struct. Dynam. 26 (1997) 1091–1112, https://doi.org/10.1002/(SICI)1096-9845(199711)26:11%3C1091::AID-EQE693%3E3.0.CO;2-6.

[48] C.E.N. Eurocode 8, in: Belgium Brussels (Ed.), Design of Structures for Earthquake Resistance—Part 3: Assessment and Retrofitting of Buildings, 2010.

[49] D.M. Aggiornamento delle, "Norme tecniche per le costruzioni" (NTC), in: Italian Ministry of Infrastructures and Transportation, 2018. Rome, Italy.

[50] Fema, Prestandard and Commentry for the Seismic Rehabilitaion of Buildings, FEMA 356, Federal Emergency Management Agency, Washington, D.C., 2000.

[51] FEMA, NEHRP guidelines for the seismic rehabilitation of buildings. Report FEMA 273, in: Federal Emergency Management Agency, 1997. Washington, DC, USA.

[52] G. Rinaldin, C. Amadio, L. Macorini, A macro-model with nonlinear springs for seismic analysis of URM buildings, Earthq. Eng. Struct. Dynam. 45 (2016) 2261–2281, https://doi.org/10.1002/eqe.2759.

[53] Y. Endo, L. Pelà, P. Roca, Review of different pushover analysis methods applied to masonry buildings and comparison with nonlinear dynamic analysis, J. Earthq. Eng. 21 (2017) 1234–1255, https://doi.org/10.1080/13632469.2016.1210055.

[54] A. Mouyiannou, M. Rota, A. Penna, G. Magenes, Identification of suitable limit states from nonlinear dynamic analyses of masonry structures, J. Earthq. Eng. 18 (2014) 231–263, https://doi.org/10.1080/13632469.2013.842190.

[55] Eurocode 8, Design of structures for earthquake resistance-part 1: general rules, seismic actions and rules for buildings, in: EN 1998-1, European Committee for Standardization, Brussels, 2005.

[56] G. Baltzopoulos, R. Baraschino, I. Iervolino, D. Vamvatsikos, SPO2FRAG: software for seismic fragility assessment based on static pushover, Bull. Earthq. Eng. 15 (2017) 4399–4425, https://doi.org/10.1007/s10518-017-0145-3.

[57] K. Beyer, E.A.I. Araya, S. Saloustros, Drift capacity models for the new masonry chapter of Eurocode 8 Part 1-2, in: R. Vacareanu, C. Ionescu (Eds.), Progresses in European Earthquake Engineering and Seismology, Springer International Publishing, Cham, 2022, pp. 398–416.

[58] M.K. Howlader, M.J. Masia, M.C. Griffith, Numerical analysis and parametric study of unreinforced masonry walls with arch openings under lateral in-plane loading, Eng. Struct. 208 (2020), 110337, https://doi.org/10.1016/j.engstruct.2020.110337.

[59] M. Peruch, E. Spacone, G. Camata, Nonlinear analysis of masonry structures using fiber-section line elements, Earthq. Eng. Struct. Dynam. 48 (2019) 1345–1364, https://doi.org/10.1002/eqe.3188.

[60] A. Aldemir, M. Altuğ Erberik, I.O. Demirel, H. Sucuoğlu, Seismic performance assessment of unreinforced masonry buildings with a hybrid modeling approach, Earthq. Spectra 29 (2013) 33–57, https://doi.org/10.1193/1.4000102.

[61] N. Mohammadgholibeyki, M. Banazadeh, The effects of viscous damping modeling methods on seismic performance of RC moment frames using different nonlinear formulations, Structures 15 (2018) 232–243, https://doi.org/10.1016/j.istruc.2018.07.009.

[62] Fema, in: United States, D.C. Washington (Eds.), Quantification of Building Seismic Performance Factors, FEMA P695, Federal Emergency Management Agency, 2009.

[63] PEER., in: PEER Ground Motion Database, University of California, Berkeley, USA, 2021. https://ngawest2.berkeley.edu/.

[64] ATC, Quantification of Building Seismic Performance Factors, FEMA P695: US Department of Homeland Security, FEMA, 2009.

[65] D. Vamvatsikos, C.A. Cornell, Applied incremental dynamic analysis, Earthq. Spectra 20 (2004) 523–553.

[66] C.A. Cornell, F. Jalayer, R.O. Hamburger, D.A. Foutch, Probabilistic basis for 2000 SAC federal emergency management agency steel moment frame guidelines, J. Struct. Eng. 128 (2002) 526–533, https://doi.org/10.1061/(ASCE)0733-9445(2002)128:4(526).

[67] J.W. Baker, Efficient analytical fragility function fitting using dynamic structural analysis, Earthq. Spectra 31 (2015) 579–599, https://doi.org/10.1193/021113eqs025m.

[68] H. Güllü, M. Karabekmez, Effect of near-fault and far-fault earthquakes on a historical masonry mosque through 3D dynamic soil-structure interaction, Eng. Struct. 152 (2017) 465–492, https://doi.org/10.1016/j.engstruct.2017.09.031.

[69] N. Simos, G.C. Manos, E. Kozikopoulos, Near- and far-field earthquake damage study of the Konitsa stone arch bridge, Eng. Struct. 177 (2018) 256–267, https://doi.org/10.1016/j.engstruct.2018.09.072.

[70] H. Güllü, F. Özel, Microtremor measurements and 3D dynamic soil–structure interaction analysis for a historical masonry arch bridge under the effects of near- and far-fault earthquakes, Environ. Earth Sci. 79 (2020) 338, https://doi.org/10.1007/s12665-020-09086-0.

[71] P. Labbé, A. Altinyollar, Conclusions of an IAEA–JRC research project on the safety significance of near-field seismic motions, Nucl. Eng. Des. 241 (2011) 1842–1856, https://doi.org/10.1016/j.nucengdes.2011.02.006.

[72] R. Dadashi, K. Nasserasadi, Seismic damages comparison of low-rise moderate reinforced concrete moment frames in the near- and far-field earthquakes by a probabilistic approach, International Journal of Advanced Structural Engineering (IJASE) 7 (2015) 171–180, https://doi.org/10.1007/s40091-015-0090-9.